

Investigating the effects of 3D urban morphology on the surface urban heat island effect in urban functional zones by using high-resolution remote sensing data: A case study of Wuhan, Central China

Xin Huang^{a,b,*,1}, Ying Wang^{a,1}

^a School of Remote Sensing and Information Engineering, Wuhan University, Wuhan 430079, PR China

^b State Key Laboratory of Information Engineering in Surveying, Mapping and Remote Sensing, Wuhan University, Wuhan 430079, PR China

ARTICLE INFO

Keywords:

Surface urban heat island
Land surface temperature
3D urban morphology
Landscape
Urban functional zone

ABSTRACT

The Urban heat island (UHI) effect is an increasingly serious problem in urban areas. Information on the driving forces of intra-urban temperature variation is crucial for ameliorating the urban thermal environment. Although prior studies have suggested that urban morphology (e.g., landscape pattern, land-use type) can significantly affect land surface temperature (LST), few studies have explored the comprehensive effect of 2D and 3D urban morphology on LST in different urban functional zones (UFZs), especially at a fine scale. Therefore, in this research, we investigated the relationship between 2D/3D urban morphology and summer daytime LST in Wuhan, a representative megacity in Central China, which is known for its extremely hot weather in summer, by adopting high-resolution remote sensing data and geographical information data. The “urban morphology” in this study consists of 2D urban morphological parameters, 3D urban morphological parameters, and UFZs. Our results show that: (1) The LST is significantly related to 2D and 3D urban morphological parameters, and the scattered distribution of buildings with high rise can facilitate the mitigation of LST. Although sky view factor (SVF) is an important measure of 3D urban geometry, its influence on LST is complicated and context-dependent. (2) Trees are the most influential factor in reducing LST, and the cooling efficiency mainly depends on their proportions. The fragmented and irregular distribution of grass/shrubs also plays a significant role in alleviating LST. (3) With respect to UFZs, the residential zone is the largest heat source, whereas the highest LST appears in commercial and industrial zones. (4) Results of the multivariate regression and variation partitioning indicate that the relative importance of 2D and 3D urban morphological parameters on LST varies among different UFZs and 2D morphology outperforms 3D morphology in LST modulation. The results are generally consistent in spring, summer and autumn. These findings can provide insights for urban planners and designers on how to mitigate the surface UHI (SUHI) effect via rational landscape design and urban management during summer daytime.

1. Introduction

The world has undergone rapid urbanization in recent decades (United Nations, 2014). The transformation of surface physical and geometric properties, upward expansion, and population explosion profoundly alter the energy balance and microclimate characteristics at the local scale, leading to a series of environmental problems (Wang et al., 2016). One of which is the urban heat island (UHI) effect, i.e., the phenomenon of the temperature being higher in urban areas than the surrounding suburban/rural areas (Kalnay and Cai, 2003). The UHI effect induces heat stress and tropospheric ozone formation, which can

both act as health hazards (Gabriel and Endlicher, 2011). The temperature increase also results in increased energy bills for air conditioning, which, in turn, raises air pollution and greenhouse gas emissions (Sarrat et al., 2006). In total, 66% of the population in the world is projected to reside in urban areas by 2050 (United Nations, 2014). Hence, how to mitigate the UHI impacts has become a major concern in many related research fields.

Urban canopy layer (UCL) refers to the atmosphere between the urban roughness elements (buildings and trees), where the climate is dominated by the micro-scale effects of the site characteristics (Oke et al., 2017). Consequently, the UCL represents the part of the

* Corresponding author.

E-mail address: xhuang@whu.edu.cn (X. Huang).

¹ Xin Huang and Ying Wang are co-first authors.

atmosphere that is vital to human comfort and health. Some numerical and physical models have been developed to investigate the factors affecting UHI effects based on the understanding of the climatology of cities (Adolphe, 2001; Martilli, 2014; Oke, 1988a, 1988b; Yang et al., 2016). Such models are able to represent the urban environment continuously, and provide the guidance that planners require. On the other hand, observational approaches including field measurement and remote sensing are also effective tools in urban climate and environmental studies, since they are potential for representing the exact urban surfaces and their spatio-temporal variations (Mirzaei, 2015). The UHI effect can be assessed by either air temperature or land surface temperature (LST). Air temperature is measured mainly by meteorological stations. However, the limited and scattered meteorological station networks can provide only partial representations of temperature variations in heterogeneous urban/suburban areas. On the other hand, LST is considered to correspond closely with canopy layer UHI and has been widely used in studying the surface UHI (SUHI) effect (Weng, 2009). LST can regulate the lower-layer air temperature of the urban atmosphere. It is a primary factor in determining the surface radiation and energy exchange, the internal climate of buildings, as well as human comfort (Oke et al., 2017). It is largely recognized that satellite-based remote sensing techniques are able to provide spatially continuous coverage of LST in a time and cost-efficient manner (Weng, 2009), as well as urban morphology information (e.g., urban structure types, landscape patterns, settlement density). Therefore, LST has been widely used to investigate the relations between the SUHI effect and urban morphology indicators (e.g., land-cover/use types, landscape patterns) (Tran et al., 2017; Weng et al., 2008; Yang et al., 2017; Zhou et al., 2017a). However, a majority of the case studies have been conducted at a medium or low resolution, e.g., using Landsat images with a 30-m resolution or MODIS images with a 500- or 1000-m resolution. Due to their ground sampling distance (GSD), pixels are often mixed and composed of multiple land-cover categories, making it difficult to depict subtle and precise urban landscape and functional zones in urban areas with highly fragmented and heterogeneous landscape (Huang et al., 2018a; Zhou et al., 2017b). High-resolution remote sensing images enable researchers to obtain detailed urban morphology information, and show great potential for the comprehensive study of the relationship between urban morphology and SUHI at fine scales.

In this context, recently, a few studies have applied high-resolution remote sensing images to examine the impact of landscape patterns and land-use types on LST (Elmes et al., 2017; Li et al., 2011; Zhou et al., 2014). However, they have mainly relied on two-dimensional (2D) information, rather than three-dimensional (3D) urban morphology, although 3D expansion is a crucial characteristic of urbanization. Buildings are a key component of the urban structure and a major contributing factor to the UHI effect, since they can potentially alter the reflection and absorption of solar radiation, as well as the proliferation of heat within urban areas (Futcher et al., 2017). Despite the apparent importance of 3D building morphology on the UHI, there exist only few studies having examined the effects of 3D urban morphology on LST, including studies of sky view factor (SVF), building height, and building volume (Berger et al., 2017; Scarano and Mancini, 2017). However, these studies provide only bivariate associations between 3D urban morphological parameters and LST, and therefore, the comprehensive explanation power of these parameters on LST is still lacking. Moreover, some 3D urban morphological parameters, which play important roles in radiation balance schemes and ventilation (e.g., shape coefficient), have not been considered yet (Depecker et al., 2001). It can be said that the relationship between LST and the high-resolution 3D urban landscape has not been sufficiently investigated.

In addition to surface cover and surface geometry, urban morphology also comprises a series of functional zones related to various human activities. Previous research has attempted to investigate how LST (or air temperature) varies with spatial patterns in urban areas (Li et al., 2016; Wong et al., 2016). One of the most widely used

classification scheme is the local climate zone (LCZ) (Stewart and Oke, 2012). It is developed to characterize the form and function of cities for UHI studies and it has been applied in remote sensing studies (Bechtel et al., 2015, 2016). Recently, some studies have sought to identify how well LCZs are separated in terms of LSTs (Cai et al., 2017; Geletič et al., 2016; Wang et al., 2018; Yang et al., 2018). Nevertheless, these studies only evaluated the thermal behavior of different LCZs (e.g., temperature differences between LCZs, temporal dynamics of cooling and warming rates of LCZs), and did not analyze the relative contributions of influential factors to LST. Moreover, the LCZ classification system normally puts more emphasis on the climate-related factors (i.e., surface structure and cover). Human activities, such as residence, production, entertainment, and education, are not sufficiently characterized by LCZs. The urban functional zone (UFZ) classification scheme is semantically abstracted from urban land used and can be used to describe human activities. UFZs are designated by physical characteristics together with social and economic functions (Zhang et al., 2017a), and have different surface properties (e.g., structure, cover, fabric), and energy consumptions, resulting in their distinct thermal regimes. Notably, UFZs can serve as the basic units for urban planning (Bateman et al., 2013). In the current literature, there have, as yet, been few attempts to comprehensively investigate the influence of UFZs on LST at a fine scale, in spite of their significance on environmental implications and planning practices. This is partly due to the difficulties in accurately identifying UFZs in urban areas. In this research, by taking advantage of high-resolution remote sensing images and geographic information data (point of interest (POI) data, Baidu street map data, road network data), the physical and socioeconomic features could be characterized more effectively, making it possible to obtain subtle UFZs over a large scale.

In summary, this study aimed to comprehensively investigate the relationship between 2D/3D urban morphology and the SUHI effect in urban functional zones using high-resolution remote sensing images, as well as 3D geographical information data. The study focused on the daytime in summer since the SUHI intensity and footprint together with its adverse effects on environment and human health have been found to be more intense during summer daytime (Peng et al., 2012; Yang et al., 2019). In addition, the stability and variations of the relationships in the other three seasons have been examined. As part of this, the following research questions are tackled by this work:

- (1) How do UFZs relate to LST variations?
- (2) How does 3D urban morphology affect LST?
- (3) What are the influences of 2D and 3D urban morphology on the LST in different UFZs?

The results of this study can help us to understand the relationship between 3D urban morphology and the SUHI effect, and can provide suggestions for urban planners and policy makers on how to ameliorate the urban thermal environment during summer daytime through rational landscape design and urban management.

2. Study area and data

2.1. Study area

Wuhan, the capital of Hubei province in China, is situated on the eastern Jiangnan Plain at the confluence of the Yangtze River and Han River, at latitude 30°35' N and longitude 114°17' E (Fig. 1a). The city of Wuhan covers approximately 8569 km², and Wuhan had a population of 10.61 million in 2015 (NBSC, 2016). Wuhan is characterized by a humid subtropical climate and suffers from extremely hot and humid summers (Peel et al., 2007). The average annual precipitation is 1260.6 mm and the average daily temperature ranges from 4.0 °C (January) to 29.1 °C (July). The city is dotted with lakes, and water accounts for a quarter of the total area. Wuhan is commonly known as

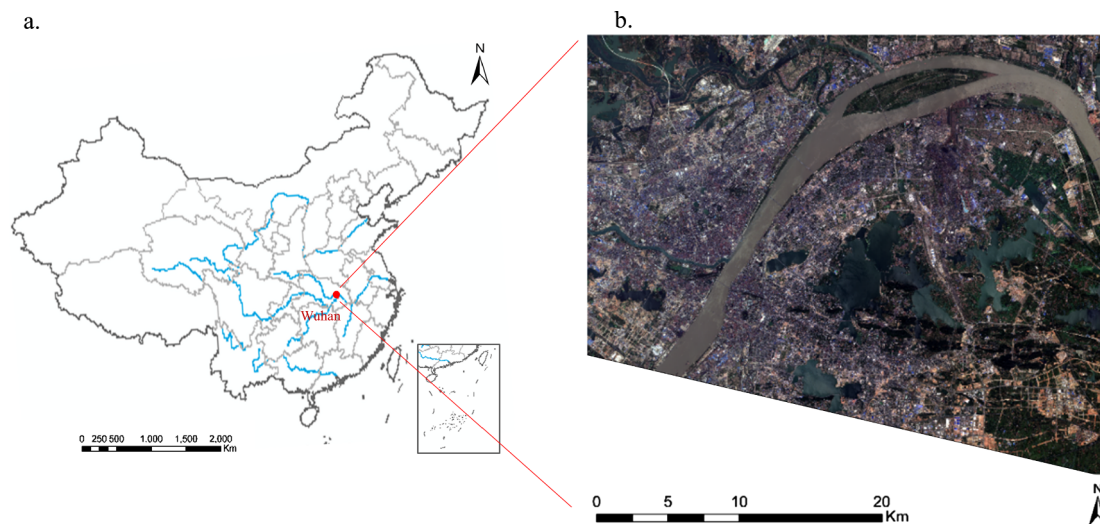


Fig. 1. Study area. (a) The location of Wuhan. (b) ZY-3 high-resolution remote sensing image (with a spatial resolution of 2.1 m) of the study area.

one of the “Four Furnaces of China”. It is a center for industry, the economy, education, and transportation in Central China, and has been witnessing rapid urbanization over the past few decades (Ali and Zhao, 2008). Given its climatic and socioeconomic characteristics, Wuhan was an ideal city to carry out this study. Our study focused on the city core of Wuhan, covering 982.6 km² (Fig. 1b).

2.2. Data

The ZiYuan-3 (ZY-3) satellite, launched in January 2012, is the first high-resolution civilian stereo mapping satellite in China. It was designed with a swath width of 50 km, which enables it to cover a relatively large area. The GSD is 2.1 m for the nadir panchromatic camera, and 5.8 m for the multispectral scanner, respectively (Huang et al., 2017). Landsat-8 images were utilized to derive the LST. Furthermore, a geographic information data set was used to facilitate the classification and analysis, including 3D building data, road network data, and POI data. The 3D building data were provided by the Wuhan Land Resources and Planning Bureau, including information on building footprint and height. Road network data were collected from OpenStreetMap. In addition, more than 130,000 POIs were acquired from a Chinese social network (Sina Weibo), containing location and functional properties of a site (e.g., community buildings, convenience stores, supermarkets, recreation facilities, restaurants, factories, museums, airports, parks). A data summary is provided in Table 1.

Table 1
Data used in this study.

Data		Resolution	Time (Mon/DD/YY)	Usage
Remote sensing data	ZY-3	2.1 m	8/12/2013	Mapping land cover and UFZs
	Landsat-8	Multispectral: 30 m; Thermal:100 m	4/26/2013; 5/12/2013 7/31/2013; 8/16/2013 9/17/2013; 10/3/2013 1/23/2014	LST retrieval
	Google Earth	/	2013	Reference of sample selection for mapping and accuracy assessment
Geographical information data	3D buildings	Vector	2013	Land-cover mapping and 3D landscape description
	Road networks	Vector	2016	Land-cover mapping and image segmentation
	POI	Vector	2014	UFZ mapping

3. Methods

3.1. Retrieval of land surface temperature

Seven cloud-free Landsat-8 images were applied for the LST retrieval: April 26, 2013 and May 12, 2013 for spring, July 31, 2013 and August 16, 2013 for summer, September 17, 2013 and October 3, 2013 for autumn, and January 23, 2014 for winter (only one image scene was available in winter during that time due to the cloud coverage). The Thermal infrared sensor (TIRS) bands have been resampled to 30 m using the cubic convolution algorithm by the U.S. Geological Survey (USGS, 2016). In this research, LSTs were estimated using the radiative transfer equation (RTF) method by correcting atmospheric effects and land surface emissivity (Sobrino et al., 2004):

$$L_{\lambda} = [\varepsilon B(T_s) + (1 - \varepsilon)L_d^{\downarrow}] \tau + L_{\mu}^{\uparrow} \tag{1}$$

where L_{λ} is the top of atmosphere (TOA) radiance, i.e., the radiance measured by the sensor. ε is the land surface emissivity which was estimated according to Dash et al. (2002) and Xie et al. (2012). T_s refers to the LST, and $B(T_s)$ is the emitted radiance from the Earth’s surface, namely, surface-leaving radiance (L_T). L_d^{\downarrow} and L_{μ}^{\uparrow} is the downwelling and upwelling atmospheric radiance, respectively. τ is the atmospheric transmissivity. The parameters L_d^{\downarrow} , L_{μ}^{\uparrow} , and τ can be obtained from the NASA Atmospheric Correction Parameter Calculator (Barsi et al., 2005).

The surface-leaving radiance (L_T) can be derived by inversion of Planck’s law:

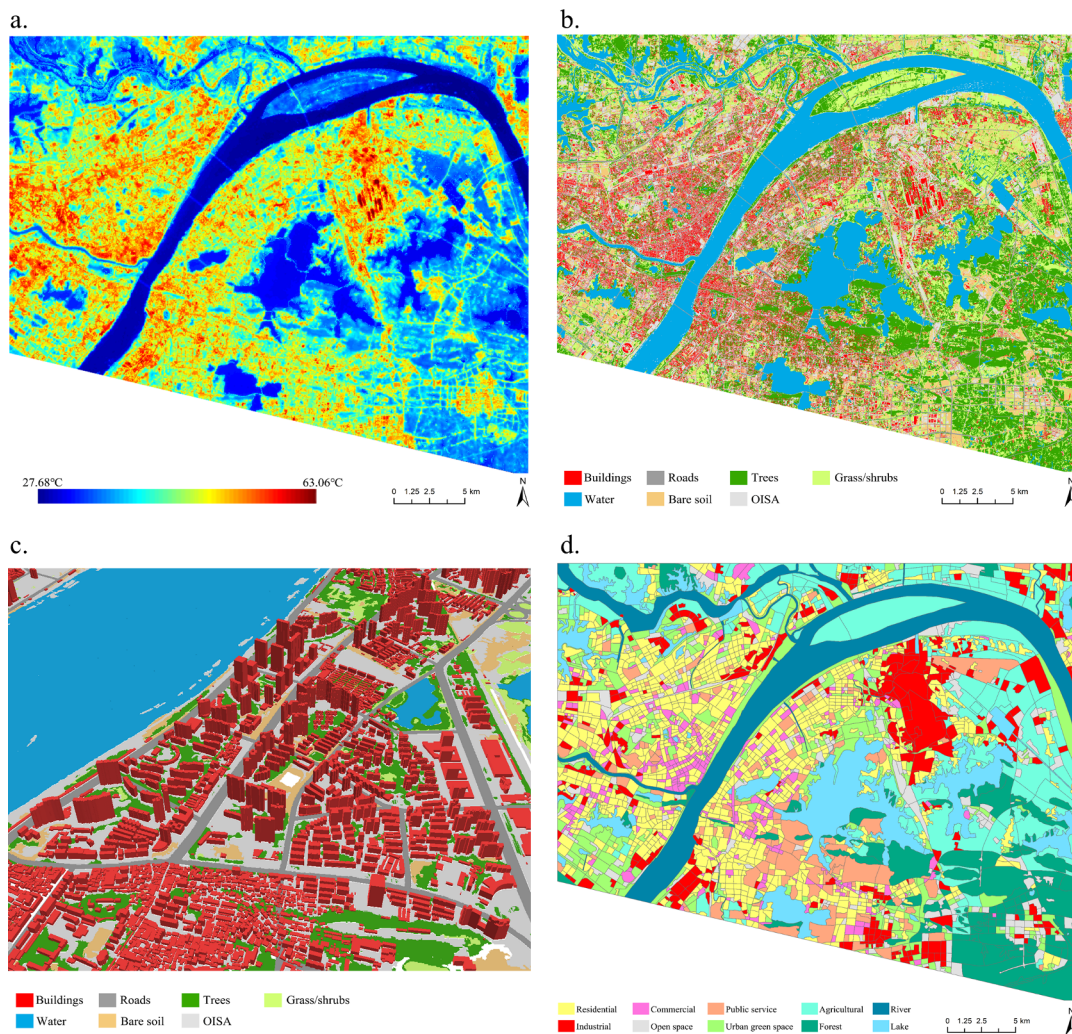


Fig. 2. (a) LST in summer. (b) Land-cover map. (c) Oblique view of the 3D land cover dataset in a sample case. (d) Urban functional zone map.

$$L_T = \frac{L_\lambda - L_\mu^\downarrow - \tau(1 - \varepsilon)L_d^\downarrow}{\tau\varepsilon} \quad (2)$$

After that, the surface-leaving radiance (L_T) was transformed to at-satellite brightness temperature (T_B), i.e., the effective brightness temperature measured by the sensor, under the assumption that the earth surface is a black body:

$$T_B = \frac{K_2}{\ln(K_1/L_T + 1)} \quad (3)$$

for TIRS band 10, K_1 is $774.89 \text{ W}/(\text{m}^2 \text{ sr } \mu\text{m})$ and K_2 is 1321.08 K .

Finally, the LST (T_s) could be calculated with corrections for land surface emissivity:

$$T_s = \frac{T_B}{1 + (\lambda T_B / \rho) \ln \varepsilon} \quad (4)$$

where λ refers to the wavelength of emitted radiance ($10.9 \mu\text{m}$ for TIRS band 10), $\rho = 1.438 \times 10^{-2} \text{ mK}$. More details about LST retrieval can be found in the studies of Weng (2009) and USGS (2016).

To make the relationships more convincing and robust, the two LSTs acquired for each season (except winter) were averaged. An example of the resulting LST is shown in Fig. 2a.

3.2. Mapping of land cover and urban functional zones

Data fusion classification is able to yield better performance than the corresponding single-source technique (Huang et al., 2018b). In this

study, multisource data (ZY-3 image, building footprint, OSM road networks) was integrated to extract seven land cover categories: buildings, roads, trees, grass/shrubs, water, bare soil, and other impervious surface areas (OISA) (e.g., squares, open areas, pavements). Building footprint and road network data were firstly used as mask layers to extract buildings and roads. For the other land-cover types, an object-oriented approach was employed due to its superiority over pixel-based classification (Blaschke et al., 2014). The proposed classification scheme consists of three steps: (1) multiresolution segmentation; (2) object-specific feature calculation (e.g., brightness, normalized difference vegetation index (NDVI), normalized difference water index (NDWI), size, hue); and (3) supervised classification. A detailed scheme is provided in Supplementary Fig. S1. Fig. 2b presents the resulting land-cover map. An oblique view of the derived 3D urban land cover in a sample case is presented in Fig. 2c.

The UFZ is an area of similar social and economic functions. It is delineated not only by its spectral and structural features extracted from high-resolution remote sensing images, but also by its socio-economic functions derived from geographic information data (Zhang et al., 2017a). In this study, 10 UFZ categories were established in consideration of both the ecological impacts of different socioeconomic activities and the national standards for land-use classification: residential, industrial, commercial, open space, public service, urban green space, agricultural, forest, river, and lake, as described in Table 2 (MLR, 2017; Zhang et al., 2017a). Residential, industrial, commercial, open space, and public service zones were defined as built-up functional

Table 2
Description of the urban functional zone categories.

Category	Description
<i>Built-up functional zones</i>	
Residential	Housing, community, and ancillary facilities, including villas, ordinary residential districts, and urban villages.
Industrial	Light industries such as electronics manufacture, food processing, and pharmaceuticals, and heavy industries such as metallurgical, steel, chemical, and machine manufacture. In addition, warehouses also belong to the industrial zone.
Commercial	Financial centers, shopping malls, retail centers, service buildings, etc.
Open space	Under-construction sites, open spaces, stations, railroads, etc.
Public service	Cultural and sports services, hospital and sanitary facilities, municipal administration buildings, educational and research institutions, etc.
<i>Non-built-up functional zones</i>	
Urban green space	Urban parks, shrubs, botanic gardens and zoos, and other urban grasslands.
Agricultural	Vegetable fields, croplands, orchards, nurseries, and other agricultural land.
Forest	Trees with distinct canopy textures.
River	The Yangtze River and its branches.
Lake	Lakes, reservoirs, ponds, etc.

zones, as they are dominated by artificial buildings and structures, and the other five UFZs were labeled as non-built-up zones (MLR, 2017). The ZY-3 image was segmented with the aid of the road network, leading to a total of 3194 city blocks (Fig. 2d). The normalized kernel densities of the POIs for each UFZ were then extracted according to Hu et al. (2016). After that, the category of each block was identified through analysis of the POI density, with the aid of visual interpretation based on high-resolution satellite images (ZY-3 and Google Earth images), in-situ images acquired by Baidu street view, and our own knowledge of the study area (Fig. 2d).

The accuracy assessment of the classified land cover map was performed via random sampling, and 100 pixels per class were chosen. Similarly, 630 blocks were randomly generated for assessing the accuracy of the UFZ map. The reference samples were labeled through visual inspection (referring to the high-resolution images from ZY-3 and Google Earth) and field verification. The classification confusion matrices are provided in Supplementary Tables S1 and S2. The overall accuracy is 93.0% for the land cover and 94.3% for the UFZs, showing reliable classification results.

3.3. 2D/3D urban landscape metrics

In this research, five widely used landscape metrics were applied to measure the urban landscape patterns (Table 3): percentage of landscape area (PLAND), edge density (ED), patch density (PD), the landscape shape index (LSI), and the patch cohesion index (COHESION) at the class level. These metrics can be used to describe the urban landscape from three aspects: area proportion (PLAND), shape complexity (ED, LSI), and spatial arrangement (PD, COHESION). All of the aforementioned metrics were calculated in FRAGSTATS 4.2 (McGarigal et al., 2002). In addition, to focus on the 2D/3D building structures, seven metrics (Table 4) involving shape, arrangement, composition, and distribution were computed. In particular, the building orientation

was defined as the angle between the major axis of the minimum enclosing rectangle of the building footprint and the x-axis, with reference to the street orientation (Ali-Toudert and Mayer, 2006). The SVF in this study refers to the ground SVF (Chun and Guldmann, 2014) and it was calculated using the Relief Visualization Toolbox in 32 directions (Zakšek et al., 2011), with a search radius of 210 m as suggested by (Chen et al., 2010). These metrics were selected as they may have potential impacts on LST (Leitão et al., 2012). Fig. 3 presents the building height and SVF in a sample area.

3.4. Statistical analysis

Firstly, one-way analysis of variance (ANOVA) was conducted to examine whether LST was significantly different among the UFZs (Li et al., 2013). Considering the possible correlations among explanatory variables (e.g., landscape composition and configuration), a partial Pearson correlation analysis was employed to investigate the correlations between the landscape variables and LST, by controlling for the interactions among them. In this research, city blocks were used as the basic analytical units. Landscape composition (PLAND) and configuration (PD, ED, LSI, COHESION, AWMSI, and OV) metrics were considered as controlled variables mutually. The 2D building metrics were also considered as controlled variables for the 3D building metrics.

The LST is determined not by a single urban morphological parameter, but by the comprehensive effect of various factors. Therefore, a stepwise multivariate linear regression analysis was then conducted to explore the relative contributions of the variables to LST. Independent variables with statistical significance ($p < 0.05$) were selected automatically via forward-backward stepwise regression (Miller, 2002). Furthermore, variation partitioning was conducted to quantify the explanatory power of 2D and 3D urban morphology in relation to LST (Borcard et al., 1992). Variation in LST was partitioned by partial regression, as implemented in the R statistical package (Buttigieg and

Table 3
Landscape metrics selected in this study.

Metrics	Abbreviation	Calculation	Description
Percentage of landscape	PLAND	$100 \times \sum_{j=1}^n a_{ij}/A$	Measures the proportional abundance of each class in the landscape.
Edge density	ED	$\sum_{k=1}^m e_{ik}/A \times 10,000$	Measures the shape complexity and isolation degree.
Patch density	PD	$n_i/A \times 10,000$	Measures the density and fragmentation.
Landscape shape index	LSI	$0.25 \sum_{k=1}^m e_{ik}^*/\sqrt{A}$	Measures the shape irregularity of patches.
Patch cohesion index	COHESION	$\left[1 - \frac{\sum_{j=1}^n p_{ij}^*}{\sum_{j=1}^n p_{ij} \sqrt{a_{ij}^*}} \right] \times \left[1 - \frac{1}{\sqrt{Z}} \right]^{-1} \times (100)$	Measures the connectivity of habitat as perceived by organisms dispersing in the landscape.

a_{ij} = area of patch ij ; e_{ik} = total length of edge in landscape involving class i , including landscape boundary and background segments involving class i ; n_i = number of patches in the landscape for class i ; e_{ik}^* = total length of edge in landscape between classes i and k , includes the entire landscape boundary and some or all background edge segments involving class i ; A = total landscape area; p_{ij}^* = perimeter of patch ij in terms of the number of cell surfaces; a_{ij}^* = area of patch ij in terms of the number of cells; Z = total number of cells in the landscape.

Table 4
Building characteristic metrics considered in this study.

Metrics	Description
2D Orientation variance (OV)	Variation of the buildings' orientations. It measures the arrangement complexity
Area-weighted mean shape index (AWMSI)	Shape complexity of an individual building. It is equal to the patch perimeter divided by the square root of the patch area
3D Shape coefficient (SC)	The ratio between the external surfaces and the volume of the building (Depecker et al., 2001). It measures the heat exchange capacity of the building with the surrounding environment
Mean height (MH)	Mean building height in a block, which represents the 3D roughness
Height variance (HV)	Height variation of buildings within a block
Normalized height variance (NHV)	The ratio between the standard deviation of building height and the mean building height. It measures the relative height variance
Sky view factor (SVF)	The fraction of the overlying hemisphere occupied by the sky, ranging from 0 (no sky visible) to 1 (no horizon obstructions visible). It measures the extent of the 3D open space

Ramette, 2014), leading to four components, i.e., unique effect of: (i) 2D urban morphology; (ii) 3D urban morphology; (iii) joint effects of 2D and 3D urban morphology; and (iv) unexplained variation. Please note that the joint effect here is the intersection of the amount of variation in the LST that could be explained by both explanatory variable groups (Borcard et al., 1992).

4. Results

4.1. Spatial pattern of urban functional zoning and LST

Given that the SUHI intensity as well as the footprint has been found to be more intense during summer daytime (Peng et al., 2012; Yang et al., 2019), this study will investigate the influence of 3D urban morphology on the SUHI effect in summer daytime and examine the stability and variations of the relationships in the other seasons.

It can be seen from Fig. 2a that high LST in summer is mainly distributed in the central and western regions, and is assembled with buildings, while the low LST is concentrated in lakes and rivers. ANOVA F-test ($p < 0.05$) indicated that significant differences exist in the LSTs among the various UFZs (Fig. 4a). The LST was further stratified into four categories: high, sub-high, sub-low, and low, based on the Jenks natural breaks classification method (Jenks, 1977). The high temperature level that contributes the most to the SUHI was defined as the

“high temperature center” (HTC). The distribution index (DI) was utilized to quantify the contribution of each UFZ type to the entire thermal environment (Eq. (5)) (Mottet et al., 2006):

$$DI = \frac{S_{hi}}{S_i} / \frac{S_h}{S} \tag{5}$$

where S_{hi} and S_i refer to the HTC area and total area in the i th UFZ, and S_h and S are the HTC area and total area in the entire study area. If the DI is larger than 1, implying that the proportion of the HTC area in the i th UFZ is higher than that in the study area, signifying that this type of UFZ is the heat source to the thermal environment (Li et al., 2017).

When looking at the proportions of the four LST categories among the UFZs in the study area (Fig. 4b), it can be observed that the HTCs are dominant in the five built-up functional zones (i.e., residential, industrial, commercial, open space, and public service), accounting for 91.3% of the total HTC area. The built-up functional zones are primarily heat sources composed of high (55.7%) and sub-high (40.0%) level LST, with DI values larger than 1, indicating their significant contribution to the SUHI effect. The commercial zone shows the highest mean LST (50.52 ± 3.68 °C), followed by industrial (50.45 ± 4.19 °C), open space (48.88 ± 4.23 °C), residential (48.67 ± 3.76 °C), and public service (46.49 ± 4.06 °C) zones. The residential zone contributes the most to the HTC area of Wuhan (37.8%, $DI = 1.71$), followed by industrial (22.7%, $DI = 2.27$) and open space (12.4%, $DI = 1.99$) zones.

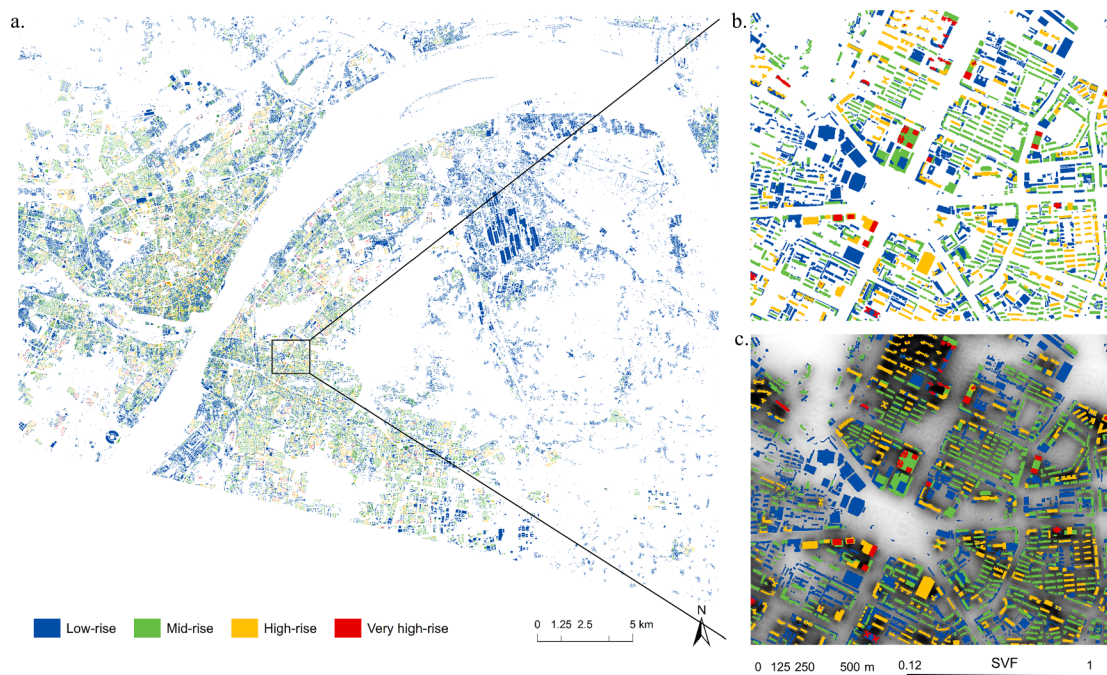


Fig. 3. (a) Building height distribution of Wuhan. The buildings were stratified into four classes according to the “Chinese code for design of civil buildings”: low-rise (< 10 m), mid-rise (10–24 m), high-rise (24–90 m), and very high-rise (> 90 m). (b) Building height and (c) SVF in a sample area.

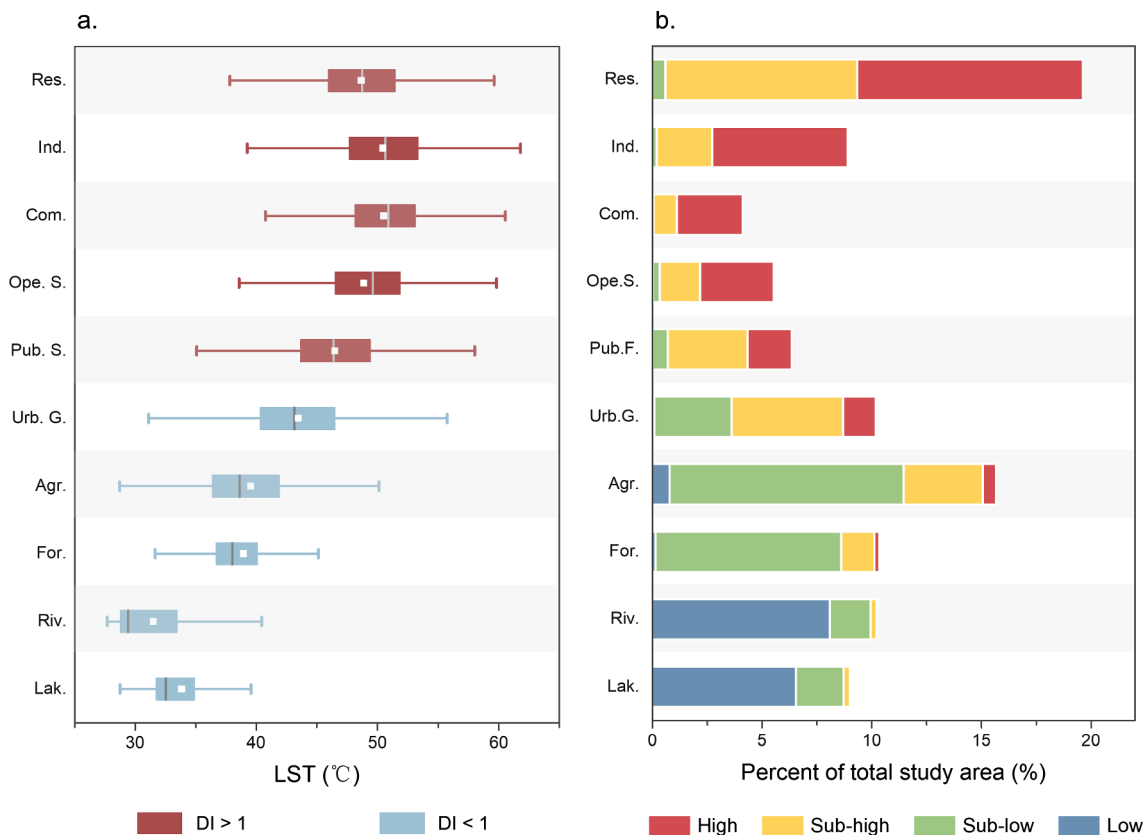


Fig. 4. LST characteristics of the different UFZs. (a) Box and whisker plots of LST for the UFZs. The square and line within the box indicate the mean and median values, respectively. (b) Stack column of the proportion of LST categories among the UFZs. (Res.: residential; Ind.: industrial; Com.: commercial; Ope. S.: open space; Pub. S.: public service; Urb. G.: urban green space; Agr.: agricultural; For.: forest; Riv.: river; Lak.: lake). (For interpretation of the references to colour in this figure legend, the reader is referred to the web version of this article.)

Although the commercial zone has the highest mean LST and DI value (2.38), it has a limited effect (11.0%) due to its small area.

Water areas feature the lowest LST. The coolest UFZs are river ($31.48 \pm 4.07 \text{ }^\circ\text{C}$) and lake ($33.83 \pm 3.12 \text{ }^\circ\text{C}$), which make up 93.2% of the low-level LST area, signifying that water areas are heat sinks which play the most significant role in dissipating heat in Wuhan. Lower mean LSTs also occur in vegetation-dominant zones. The urban green space, agricultural, and forest zones constitute the main sub-low LST category (79.4%). The LST in the urban green space zone ($43.47 \pm 4.39 \text{ }^\circ\text{C}$, $DI = 0.48$) is significantly higher than that in the agricultural zone ($39.52 \pm 4.11 \text{ }^\circ\text{C}$, $DI = 0.13$) and forest zone ($38.94 \pm 3.33 \text{ }^\circ\text{C}$, $DI = 0.07$).

4.2. Correlation between urban morphological parameters and LST

The correlations between the landscape metrics (as shown in Tables 5 and 6) and summer LST of the built-up functional zones were

Table 5

Partial Pearson correlation coefficients between the 2D landscape metrics and LST of the built-up functional zones. For the composition metric (PLAND), the controlled variables were the configuration metrics (PD, ED, LSI, COHESION, AWMSI, OV), and for the configuration metrics, composition metric was considered as the controlled variable.

	PLAND	PD	ED	LSI	COHESION	AWMSI	OV
2D buildings	0.291**	-0.376**	-0.257**	-0.211**	0.225**	0.099**	0.007
OISA	0.177**	0.300**	0.322**	0.173**	0.083**	-	-
Grass/shrubs	-0.190**	-0.324**	-0.225**	-0.179**	-0.105**	-	-
Trees	-0.231**	0.004	-0.014	-0.013	-0.084**	-	-
Bare soil	-0.023	-0.090**	0.094**	-0.054*	-0.101**	-	-

* $P < 0.05$ (2-tailed).
 ** $P < 0.01$ (2-tailed).

Table 6

Pearson correlation coefficients between the 3D building metrics and LST of the built-up functional zones. The italic row is the partial Pearson correlation coefficients, where the 2D building morphological parameters were considered as controlled variables.

	SC	MH	HV	NHV	SVF
3D buildings	-0.136**	-0.106**	-0.014	0.112**	-0.156**
	<i>0.034*</i>	<i>-0.142**</i>	<i>-0.107**</i>	<i>0.002</i>	<i>0.135**</i>

* $P < 0.05$ (2-tailed).
 ** $P < 0.01$ (2-tailed).

examined due to their dominant proportions of heat sources. Table 5 illustrates the partial correlation coefficients between the LST and 2D landscape metrics. LST is correlated with all the landscape metrics for OISA and grass/shrubs. For OISA, all the correlations are positive, showing its warming effect. Positive correlations of ED_OISA (partial

$r = 0.322$, $P < 0.01$) and PD_OISA (partial $r = 0.300$, $P < 0.01$) indicate that a fragmented and isolated distribution for OISA may lead to an increasing tendency for LST. The inverse trend is found for grass/shrubs, with all the landscape metrics negatively associated with LST, especially PD_Grass/shrubs (partial $r = -0.324$, $P < 0.01$), ED_Grass/shrubs (partial $r = -0.225$, $P < 0.01$), and PLAND_Grass/shrubs (partial $r = -0.190$, $P < 0.01$), implying that a dispersed distribution and irregular shape for grass/shrubs can help to mitigate the SUHI effect. As for trees, only landscape composition (PLAND_Trees) is significantly correlated with LST (partial $r = -0.231$, $P < 0.01$). The bare soil does not show much association with LST.

Results reveal that buildings have a complex impact on LST. PLAND_Buildings (partial $r = 0.291$, $P < 0.01$) and COHESION_Buildings (partial $r = 0.225$, $P < 0.01$) are significantly positively related to LST, while PD_Buildings (partial $r = -0.376$, $P < 0.01$), ED_Buildings (partial $r = -0.257$, $P < 0.01$), and LSI_Buildings (partial $r = -0.211$, $P < 0.01$) are negatively related to LST. It can be inferred that areas with intensive, connected, and aggregated buildings tend to suffer from higher LST. As for the 3D building metrics, the correlations are weaker than that for the 2D ones (Table 6). The LST is found to have positive relationship with NHV_Buildings ($r = 0.112$, $P < 0.01$) and negative relationships with SVF_Buildings ($r = -0.156$, $P < 0.01$), SC_Buildings ($r = -0.136$, $P < 0.01$) and MH_Buildings ($r = -0.106$, $P < 0.01$). While after controlling for the effect of 2D building morphological parameters, partial correlation coefficients demonstrate that three out of the five 3D building metrics are significantly related to LST: MH_Buildings (partial $r = -0.142$, $P < 0.01$), SVF_Buildings (partial $r = 0.135$, $P < 0.01$), and HV_Buildings (partial $r = -0.107$, $P < 0.01$). It is interesting to find that SVF_Buildings has an inverse trend after considering the effect of 2D building morphological parameters.

4.3. Relative importance of urban morphology for LST

Furthermore, the 2D and 3D urban morphological parameters were modeled using multivariate stepwise linear regression to examine the relative contribution of each variable to LST in the built-up functional zones. Table 7 lists the outcome of the multivariate regression analysis. Variation partitioning was further employed to explore the independent and joint explanatory power of variable groups by decomposing the variation in LST into four fractions (see Section 3.4). To explore the influential factors with respect to different UFZs, the models for the four functional zones (residential, industrial, commercial, and public service) were separately constructed.

In the general model, it can be seen that approximately 69.4% of the variation in LST can be explained by the 15 variables. PLAND_Trees ($\beta = -0.511$) and PLAND_Grass/shrubs ($\beta = -0.349$) outperform all the other factors in reducing LST. Buildings play a prominent role in the LST magnitude. In particular, LST can be reduced with an increase of MH_Buildings ($\beta = -0.238$) and decrease of PLAND_Buildings ($\beta = 0.154$) and ED_Buildings ($\beta = 0.148$). Results from the variation partitioning indicate that the largest proportion in LST is accounted for by the unique effect of the 2D urban morphological parameters (fraction i, 58.2%) (Fig. 5). The unique effect of 3D urban morphological parameters (fraction ii, 4.1%) and joint effect of the 2D and 3D urban morphological parameters (fraction iii, 6.8%) make limited contributions (Fig. 5).

With respect to the four separate models in terms of different UFZs, the variables considered above can explain 59.7–73.2% of the variance in LST. LST is influenced mostly by the 2D and 3D building morphological parameters, composition of trees and grass/shrubs, and PD_Grass/shrubs. PLAND_Trees has the most notable effect in all the zones. The contributions of building morphological parameters are different among the UFZ types. Specifically, in the residential zone, 3D morphology (MH_Buildings, $\beta = -0.222$) plays the most important role. Whereas in the industrial area, 2D morphology (PLAND_Buildings,

$\beta = 0.296$, and LST_Buildings, $\beta = 0.235$) has an overriding effect. In the commercial zone, ED_Buildings ($\beta = 0.267$), SVF_Buildings ($\beta = 0.208$), and MH_Buildings ($\beta = -0.197$) make prominent contributions. In the public service zone, HV_Buildings ($\beta = -0.209$), SVF_Buildings ($\beta = -0.194$), and NHV_Buildings ($\beta = 0.152$) are the most important building morphological parameters.

In the case of variation partitioning (Fig. 5), the independent effect of the 2D landscape variables dominates the LST variation in the four UFZs (fraction i, 46.1–59.8%). Variables pertaining to 3D building morphology independently capture 5.2% of the LST variation in the commercial zones. In the other zones, the independent contribution of 3D building morphology is relatively little, but the joint effects of 2D and 3D morphology are noteworthy (fraction iii, 15.6%, 18.6%, and 9.7% for the residential, industrial and public service zones). The results offer insights into the contribution of different variable groups to the LST, indicating that 2D urban morphology outperforms 3D morphology in LST modulation and LST variability cannot be predicted well with 3D urban morphological parameters alone.

5. Discussion

5.1. Influence of 2D/3D urban morphology on LST

According to the theory of the “urban energy balance”, when the horizontal heat advection is not considered, the energy absorbed by the surface from solar radiation and that generated by anthropogenic activities is balanced by heating up the air above the surface (via convection and radiation), evapotranspiration, as well as heat storage in surface materials (Oke, 1988b). The urban morphology can affect the partitioning of this energy balance and can therefore modify the urban microclimate. This study reveals that the summer HTCs in Wuhan are most often found in built-up functional zones. Overall, four land-cover classes have a major impact on intra-urban LST variation at a fine scale during summer daytime: buildings, OISA, grass/shrubs, and trees.

The proportion of trees is the most important cooling factor to LST (Tables 5 and 7), which is well in line with previous studies (Elmes et al., 2017; Peng et al., 2014; Weng et al., 2004). Trees help reduce LST primarily by evapotranspiration and blocking of solar radiation from directing heating of the surface through casting shade (Oke et al., 1989). In this research, however, we found few significant correlations between LST and the spatial configuration of trees, which differs from the findings of some other studies (Maimaitiyiming et al., 2014; Zhang et al., 2017b). The possible reason is that aforementioned studies did not consider the effect of the proportion of trees when quantifying the relationship between their spatial configuration and LST. On the one hand, the increase in ED and LSI may increase the shade provided by trees and enhance the interface between trees and surrounding built-up areas (e.g., buildings, impervious surfaces), which may favor LST reduction by shading effect and convective heat loss (Zhao et al., 2014). On the other hand, given the same area of trees, the increase in ED and LSI is accompanied with more fragmented patches, resulting in a reduced canopy density and evapotranspiration efficiency, which may lead to higher LST (Shahidan et al., 2012). Consequently, the changes in LST caused by the increase in ED and LSI largely depend on the net effects of the aforementioned two processes. Please note that, the magnitude of LST changed by shading may be larger than evapotranspiration since shading directly impacts the temperature of the surroundings. Hence, how to locate urban trees to maximize their benefits from the joint effect of shading and evapotranspiration is an important concern for urban design. Compared to trees, the relationships between landscape configuration of grass/shrubs and LST are statistically significant, although their contribution is less than that of trees. Our results demonstrate that the increase in PD and ED of grass/shrubs may decrease LST. The possible reason is that urban areas are characterized by a mosaic landscape dotted with heat sources (e.g., impervious surfaces, buildings) and heat sinks (e.g., grassland, trees,

Table 7
Regression result of LST and the urban morphological parameters. R^2 represents the proportion of the LST variation that can be explained by the regression model, and β represents the relative contribution of each variable to LST.

	General	Residential	Industrial	Commercial	Public Service
<i>2D building</i>					
PLAND	0.154	0.172	0.296	0.180	
PD	-0.048				
ED	0.148			0.267	
LSI			0.235		
COHESION	0.046	0.088			
<i>3D building</i>					
MH	-0.238	-0.222		-0.197	
HV					-0.209
NHV					0.152
SVF				0.208	-0.194
<i>OISA</i>					
PLAND	0.108				0.225
PD	0.086	0.106			0.133
ED	-0.181				
LSI	0.152			0.078	
<i>Grass/shrubs</i>					
PLAND	-0.349	-0.435	-0.298	-0.233	-0.254
PD	-0.143	-0.151	-0.268	-0.154	-0.166
ED					
LSI	-0.120				
COHESION		0.058	-0.105		
<i>Tree</i>					
PLAND	-0.511	-0.56	-0.316	-0.395	-0.565
PD	-0.084	-0.095		-0.151	
ED	0.099	0.128			
R^2	0.694	0.713	0.641	0.597	0.732
Adjusted R^2	0.691	0.711	0.635	0.587	0.720
β	-1		0		1

The color in the table indicates the value of β (as shown in the bottom of the table), where the color scales of red and blue represent high positive and negative values, respectively.

water). The transition between them is sharp, making the microscale advection vital in the UCL. Irrigated grass/shrubs are heat sinks that are usually surrounded by impervious surfaces. When hot and dry air advects across them, the heat carried by it can be a source of energy for evapotranspiration, and the dryness enhances the surface-air vapor gradient. Since irrigation supplies moisture, the evapotranspiration efficiency will not be limited (Elmes et al., 2017; Oke, 1988b). Therefore, the dispersed distribution of grass/shrubs can enhance energy flow but has little effect on evapotranspiration efficiency.

Replacement of vegetation with impervious surfaces leads to an increase of LST, which is generally consistent with the findings of previous studies (Estoque et al., 2017; Zhou et al., 2011). These materials (e.g., concrete, cement, asphalt) exhibit lower emissivity and higher heat capacity. The impervious and dry surface can reduce the evapotranspiration efficiency relative to natural land, and hence favor partitioning solar radiation into sensible rather than latent heat (Landsberg, 1981; Oke et al., 2017). However, our results further revealed the significant effect of the spatial arrangement of individual buildings on LST, i.e., compacted and concentrated forms of buildings have positive relationships with LST. Connected buildings obstruct

ventilation, which induces the trapping of heat and air pollutants. Moreover, under the circumstance of high temperature and pollutant levels, as well as poor natural air circulation, air conditioning systems may be extensively used, resulting in further heat release (Wong and Lau, 2013).

The relationship between 3D urban morphology (e.g., aspect ratio, SVF, volume of human constructions) and air temperature has been the subject of several studies (Chen et al., 2010; Wu and Lung, 2016). Our results revealed that 3D urban morphology also has an influence on LST during summer daytime, but the relationships are not as close as that for the 2D urban morphology. MH and SVF are the most significant 3D landscape metrics in our research. MH is found to have a significant negative relationship with LST in summer, which diverges from the one observed by Berger et al. (2017). High-rise buildings are capable of casting more shadows and improving the surface roughness to generate mechanical turbulence, and thereby enhances the convective heat dissipation (Li et al., 2011). This was also suggested by Zhao et al. (2014), that an increase in building height can mitigate UHI during daytime. In particular, in this study, it is interesting to find that the correlation between SVF and LST changed from negative to positive after

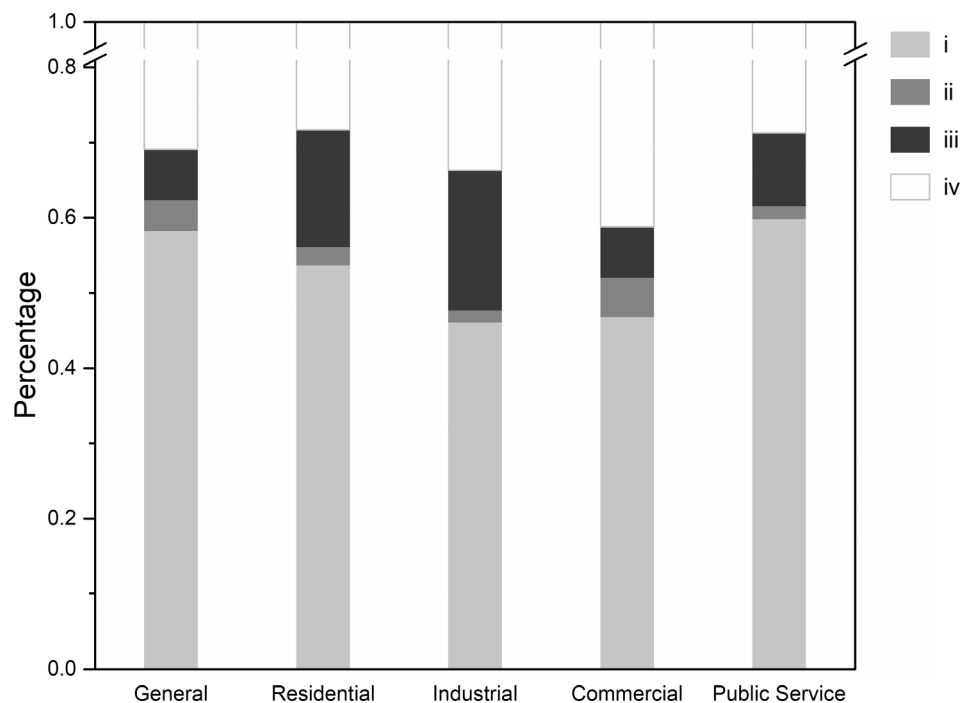


Fig. 5. The contributions (expressed as the percentage of the total explained variance) of the predictor variables for LST in urban functional zones. (i: unique effect of 2D urban morphology; ii: unique effect of 3D urban morphology; iii: joint effect of 2D and 3D urban morphology; iv: unexplained variation).

controlling for the effect of 2D building morphology. SVF can regulate the LST in two ways: ventilation and incoming solar radiation. Specifically, on the one hand, higher SVF, representing more visible open sky, can help enhance air circulation and wind speed in a densely built environment and therefore decrease the temperature (Yang et al., 2013). On the other hand, lower SVF could reduce the incoming solar radiation to penetrate into surface, and thus can help LST reduction (Jamei et al., 2016). Previous research on the issue of the relationship between SVF and temperature are, in some cases, contradictory. Both positive (Charalampopoulos et al., 2013), negative (Berger et al., 2017), and insignificant (Hove et al., 2015) relationships have been reported. This can be attributed to the relative strength of the influence of the two processes, which is associated with the local climatology, geography, and surface topology of the study sites (Zhou et al., 2017c).

The relationship between LST and urban morphology is determined by the comprehensive influence of various factors. Yet, to our knowledge, the comprehensive relationship between LST and urban morphology of different UFZs is still lacking. In this study, the results of the multivariate regression and variation partitioning in the four built-up functional zones suggest that the factors affecting LST are different in each UFZ. The statistics for the variables in the four UFZs are described in Supplementary Tables S3. The proportion of trees is the most important factor on reducing LST, and the relationship is weaker in industrial and commercial zones where PLAND_Trees are smaller with respect to the other zones. Public service zone has the lowest building density, and we found that in this zone, 2D building morphology has little effect on LST variation. Similarly, in industrial zones, which show the lowest building height, 3D building morphology presents little effect. In commercial zones, characterized by high-density and high-rise buildings, the visible open sky is rather limited. LST is positively related to SVF, indicating that shading has a larger impact in this area.

The highest LST in Wuhan is found in the commercial and industrial zones, which is consistent with previous findings (Li et al., 2011). The commercial zone has the lowest coverage of trees and grass/shrubs and the highest proportion of buildings and impervious surfaces (Supplementary Tables S3), corresponding to lower emissivity and higher heat capacity (Landsberg, 1981; Oke et al., 2017). Although the

industrial zone has more green spaces and fewer artificial surfaces, its LST is second only a little to the commercial zone. This phenomenon further suggests the complex mechanism of urban microclimate at fine scales. It is influenced not only by biophysical processes, but also by anthropogenic factors. Wuhan is a large industrial city with heavy industries such as steel, mechanical manufacturing, petrochemicals, which consume a great deal of energy and release a large amount of heat (Li et al., 2014). The explanatory power of urban morphology is relatively low in the commercial and industrial zones, implying that other factors such as energy consumption and emissions may play more important roles with regard to LST (Zhou et al., 2012).

Water areas are the coolest UFZ and can significantly reduce the LST. Vegetation dominated regions also have a crucial mitigation effect. The LST in the urban green space zone is significantly higher than that in the agricultural zone and forest zone. A possible reason is that urban green spaces are usually found in areas with a high intensity of built-up areas nearby, and are composed of a number of soil and artificial structures (e.g., trails, squares), which have low water-retention rates and specific heat capacities (Kjellgren and Montague, 1998). As a result, the soil moisture and evapotranspiration intensity are less than that in agricultural and forest areas, resulting in less heat release and more sensible heat (Kotzen, 2003).

5.2. Seasonal stability and variations of the relationships

The relationship between 2D and 3D urban morphological parameters and LST as well as the relative contributions of the parameters to LST have been also verified in spring, autumn, and winter. The results are shown in Supplementary Fig. S2 and Tables S4–S8.

Tables S4–S8 indicate that the relationship between 2D/3D urban morphological parameters and LST is generally consistent in spring, summer and autumn. However, results in winter show some variations. One of the most prominent variations is the increase in the magnitude of correlations between 3D building metrics and LST in winter. Such impact may stem from the changes in the amount of solar radiation reaching the Earth. The sun elevation in winter (34.95°) is much lower than that in summer (65.80° and 63.41°, respectively). This

circumstance is accompanied by a significant reduction in solar radiation and an increase of shadowing effect which is caused by the obstructions of vertical building walls (Theeuwes et al., 2014). The strength of correlation between 2D landscape and LST is decreased, which is well in line with the results of (Ma et al., 2016; Zhou et al., 2014). Moreover, with the reduced solar radiation, the sensible heat partitioned by impervious surfaces can be decreased. On the other hand, the metabolic activity of vegetation greatly weakens in winter. The decrease in the rate of evapotranspiration leads to a reduction in cooling. In addition, grassland has been degraded into bare soil, so that its cooling effect is barely evident. Some studies have determined that vegetation-related variables are not good factors for predicting LST in winter (Yuan and Bauer, 2007). It can be seen from Fig. 1 that the relationships between urban morphological parameters and LST is weaker in winter. Given that the SUHI intensity and footprint together with its adverse effects on environment and human health have been found to be more intense during daytime in summer (Peng et al., 2012; Yang et al., 2019), this is probably the reason that many SUHI studies focus on summer.

5.3. Implications for urban planning and management

The results of this study imply that urban morphology, including 2D urban morphology, 3D urban morphology, and UFZ have important impacts on intra-urban LST during summer daytime.

Special attention should be paid to buildings, grass/shrubs, and trees for urban planning at a fine scale. Buildings have a significant effect on LST since they determine the absorption of solar radiation, the formation of airflow, and the generation of anthropogenic heat. It is suggested that urban planners could optimize the spatial arrangement of the urban landscape by dispersing built-up surfaces. However, it is unrealistic to reduce the amount of artificial surfaces in urban areas where land resources are valuable and scarce, but we could mitigate the daytime SUHI effect by replacing the horizontal expansion of buildings with vertical extension. The distribution of trees and grass/shrubs helps to mitigate the SUHI effect via evapotranspiration and shading effect. Their proportion is an important factor for the alleviating effect. In addition, the configuration of grass/shrubs can also affect LST. Given limited available space for urban greening, interspersing grass/shrubs into urban area may be an effective way to mitigate the SUHI effect rather than concentrated distribution.

In terms of UFZs, the LST characteristics of the UFZ classes revealed by this study could help to minimize the impacts of urbanization by targeted landscape optimization and land-use planning. For instance, in the commercial and residential zones with high-density and high-rise buildings, the design of the 3D building morphology should be paid more attention to. The explanatory power of urban morphology is relatively high in the residential and public service zones, indicating that the rational planning of the urban landscape can efficiently mitigate the urban warming effect in these regions. Apart from the urban morphology, other strategies (such as modifying albedo of construction materials, green roofs and green facades) also have cooling effects on urban environment on urban environment (Aflaki et al., 2016; Kikegawa et al., 2006; Kleerekoper et al., 2012).

5.4. Limitations and recommendations for future studies

While this study has revealed the effect of 3D urban morphology on

the SUHI effect in different UFZs, there are several limitations deserving further studies. First, nighttime LST was not considered in this study since Landsat data is only available at daytime. Second, the satellite-based sensors tend to observe horizontal surfaces and may ignore the vertical walls, while the latter is important to the climate near street level, especially in densely built areas. Hence, the representation of vertical wall surfaces via satellite-based remote sensing remains limited. In future research, multiple daytime and nighttime thermal data (e.g., mid-resolution ASTER data, low-resolution MODIS data) may be included to explore the diurnal relationship between urban morphology and LST. Furthermore, we plan to conduct this research in more cities with various climatic conditions to examine the generality of the results.

6. Conclusion

This study aimed at investigating the effects of urban morphology on intra-urban LST variation, including 2D urban morphology, 3D urban morphology, and UFZs. Based on high-resolution remote sensing data and geographic information data, our results suggest the complex mechanism of the relationships between 2D/3D urban morphology and LST during summer daytime at a fine scale. Local LST is closely related to microscale landscape design characteristics. The relationships between LST and 2D/3D urban morphology were quantified using a partial Pearson correlation analysis, to control for the interactions among explanatory variables. From the landscape viewpoint, both the composition and configuration of buildings are significantly related to LST. The scattered distribution facilitates the mitigation of LST. 3D urban morphology, such as MH, SVF, is also found to affect the variation of LST. Daytime LST could be reduced with increasing building height. The influence of SVF is context-dependent, as SVF has competing effects on LST via regulating the ventilation, incoming solar radiation, as well as trapping thermal radiation. Trees are the most influential factor in reducing LST, and the cooling efficiency mostly depends on their proportions. The spatial distribution of grass/shrubs can also help to mitigate LST, and the fragmented and irregular distribution is therefore recommended.

Another contribution of this research is to reveal the different effects of urban morphology to LST in different urban function zones (UFZs). Our results show that the residential zone is the largest heat source in the urban, while the highest LST occurs in commercial and industrial zones. Vegetation and water areas form the 'cool islands' in urban areas. Results of the multivariate regression and variation partitioning indicate that the relative contribution of 2D and 3D morphological parameters in explaining the variation of LST also varies among the different UFZs. This study can provide an insight into deeper understanding of the mechanisms of the SUHI effect and provide recommendations for mitigating surface temperature during extremely hot summer daytime.

Acknowledgements

The research was supported by the National Natural Science Foundation of China under Grant 41771360, the National Program for Support of Top-notch Young Professionals, and the Hubei Provincial Natural Science Foundation of China under Grant 2017CFA029.

Appendix A. List of abbreviations

See Table A1.

Table A1
List of abbreviations.

Abbreviation	Full name
2D	Two-dimensional
3D	Three-dimensional
ANOVA	Analysis of variance
AWMSI	Area-weighted mean shape index
COHESION	Patch cohesion index
ED	Edge density
GSD	Ground sampling distance
HTC	High temperature center
HV	Height variance
LCZ	Local climate zone
LSI	Landscape shape index
LST	Land surface temperature
MH	Mean height
NDVI	Normalized difference vegetation index
NDWI	Normalized difference water index
NHV	Normalized height variance
OISA	Other impervious surface areas
PLAND	Percentage of landscape area
POI	Point of interest
SC	Shape coefficient
SUHI	Surface urban heat island
SVF	Sky view factor
UCL	Urban canopy layer
UFZ	Urban functional zone
UHI	Urban heat island
ZY-3	ZiYuan-3

Appendix B. Supplementary material

Supplementary data to this article can be found online at <https://doi.org/10.1016/j.isprsjprs.2019.04.010>.

References

- Adolphe, L., 2001. A simplified model of urban morphology: application to an analysis of the environmental performance of cities. *Environ. Plan. B: Plan. Design* 28, 183–200.
- Aflaki, A., Mirnezhad, M., Ghaffarianhoseini, A., Ghaffarianhoseini, A., Omrany, H., Wang, Z.H., Akbari, H., 2016. Urban heat island mitigation strategies: a state-of-the-art review on Kuala Lumpur, Singapore and Hong Kong. *Cities* 62, 131–145.
- Ali-Toudert, F., Mayer, H., 2006. Numerical study on the effects of aspect ratio and orientation of an urban street canyon on outdoor thermal comfort in hot and dry climate. *Build. Environ.* 41, 94–108.
- Ali, R., Zhao, H., 2008. Wuhan, China and Pittsburgh, USA: urban environmental health past, present, and future. *EcoHealth* 5, 159–166.
- Barsi, J.A., Schott, J.R., Palluconi, F.D., Hook, S.J., 2005. Validation of a web-based atmospheric correction tool for single thermal band instruments, *Optics and Photonics 2005*. SPIE, pp. 7.
- Bateman, L.J., Harwood, A.R., Mace, G.M., Watson, R.T., Abson, D.J., Andrews, B., Binner, A., Crowe, A., Day, B.H., Dugdale, S., 2013. Bringing ecosystem services into economic decision-making: land use in the United Kingdom. *Science* 341, 45.
- Bechtel, B., Alexander, J.P., Böhner, J., Ching, J., Conrad, O., Feddema, J., Mills, G., See, L., Stewart, I., 2015. Mapping local climate zones for a worldwide database of the form and function of cities. *ISPRS Int. J. Geo-Inf.* 4.
- Bechtel, B., See, L., Mills, G., Foley, M., 2016. Classification of local climate zones using SAR and multispectral data in an arid environment. *IEEE J. Sel. Top. Appl. Earth Obs. Remote Sens.* 9, 3097–3105.
- Berger, C., Rosentreter, J., Voltersen, M., Baumgart, C., Schmuilius, C., Hese, S., 2017. Spatio-temporal analysis of the relationship between 2D/3D urban site characteristics and land surface temperature. *Remote Sens. Environ.* 193, 225–243.
- Blaschke, T., Hay, G.J., Kelly, M., Lang, S., Hofmann, P., Addink, E., Queiroz Feitosa, R., van der Meer, F., van der Werff, H., van Coillie, F., Tiede, D., 2014. Geographic object-based image analysis – towards a new paradigm. *ISPRS J. Photogramm. Remote Sens.* 87, 180–191.
- Borcard, D., Legendre, P., Drapeau, P., 1992. Partialling out the spatial component of ecological variation. *Ecology* 73, 1045–1055.
- Buttigieg, P.L., Ramette, A., 2014. A guide to statistical analysis in microbial ecology: a community-focused, living review of multivariate data analyses. *FEMS Microbiol. Ecol.* 90, 543–550.
- Cai, M., Ren, C., Xu, Y., Lau, K.K.-L., Wang, R., 2017. Investigating the relationship between local climate zone and land surface temperature using an improved WUDAPT methodology – a case study of Yangtze River Delta, China. *Urban Climate*.
- Charalampopoulos, I., Tsiros, I., Chronopoulou-Sereli, A., Matzarakis, A., 2013. Analysis of thermal bioclimate in various urban configurations in Athens, Greece. *Urban Ecosystems* 16, 217–233.
- Chen, L., Ng, E., An, X., Ren, C., Lee, M., Wang, U., He, Z., 2010. Sky view factor analysis of street canyons and its implications for daytime intra-urban air temperature differentials in high-rise, high-density urban areas of Hong Kong: a GIS-based simulation approach. *Int. J. Climatol.* 32, 121–136.
- Chun, B., Guldmann, J.M., 2014. Spatial statistical analysis and simulation of the urban heat island in high-density central cities. *Landscape Urban Plann.* 125, 76–88.
- Dash, P., Götsche, F.M., Olesen, F.S., Fischer, H., 2002. Land surface temperature and emissivity estimation from passive sensor data: theory and practice-current trends. *Int. J. Remote Sens.* 23, 2563–2594.
- Depecker, P., Menezes, C., Virgone, J., Lepers, S., 2001. Design of buildings shape and energetic consumption. *Build. Environ.* 36, 627–635.
- Elmes, A., Rogan, J., Williams, C., Ratick, S., Nowak, D., Martin, D., 2017. Effects of urban tree canopy loss on land surface temperature magnitude and timing. *ISPRS J. Photogramm. Remote Sens.* 128, 338–353.
- Estoque, R.C., Murayama, Y., Myint, S.W., 2017. Effects of landscape composition and pattern on land surface temperature: an urban heat island study in the megacities of Southeast Asia. *Sci. Total Environ.* 577, 349–359.
- Futcher, J., Mills, G., Emmanuel, R., Korolija, I., 2017. Creating sustainable cities one building at a time: towards an integrated urban design framework. *Cities* 66, 63–71.
- Gabriel, K.M.A., Endlicher, W.R., 2011. Urban and rural mortality rates during heat waves in Berlin and Brandenburg, Germany. *Environ. Pollut.* 159, 2044–2050.
- Geletič, J., Lehnert, M., Dobrovolný, P., 2016. Land surface temperature differences within local climate zones, based on two central European cities. *Remote Sensing* 8, 788.
- Hove, L.W.A.V., Jacobs, C.M.J., Heusinkveld, B.G., Elbers, J.A., Driel, B.L.V., Holtslag, A.A.M., 2015. Temporal and spatial variability of urban heat island and thermal comfort within the Rotterdam agglomeration. *Build. Environ.* 83, 91–103.
- Hu, T., Yang, J., Li, X., Gong, P., 2016. Mapping urban land use by using landsat images and open social data. *Remote Sensing* 8, 151.
- Huang, X., Chen, H., Gong, J., 2018a. Angular difference feature extraction for urban scene classification using ZY-3 multi-angle high-resolution satellite imagery. *ISPRS J. Photogramm. Remote Sens.* 135, 127–141.
- Huang, X., Hu, T., Li, J., Wang, Q., Benediktsson, J.A., 2018b. Mapping urban areas in china using multisource data with a novel ensemble SVM method. *IEEE Trans. Geosci. Remote Sens.* 56, 4258–4273.
- Huang, X., Wen, D., Li, J., Qin, R., 2017. Multi-level monitoring of subtle urban changes for the megacities of China using high-resolution multi-view satellite imagery. *Remote Sens. Environ.* 196, 56–75.
- Jamei, E., Rajagopalan, P., Seyedmahmoudian, M., Jamei, Y., 2016. Review on the impact of urban geometry and pedestrian level greening on outdoor thermal comfort. *Renew. Sustain. Energy Rev.* 54, 1002–1017.
- Jenks, G.F., 1977. *Optimal Data Classification for Choropleth Maps*. University of Kansas, Lawrence, Kansas.
- Kalnay, E., Cai, M., 2003. Impact of urbanization and land-use change on climate. *Nature* 423, 528–531.

- Kikegawa, Y., Genchi, Y., Kondo, H., Hanaki, K., 2006. Impacts of city-block-scale countermeasures against urban heat-island phenomena upon a building's energy-consumption for air-conditioning. *Appl. Energy* 83, 649–668.
- Kjelgren, R., Montague, T., 1998. Urban tree transpiration over turf and asphalt surfaces. *Atmos. Environ.* 32, 35–41.
- Kleerekoper, L., Esch, M.V., Salcedo, T.B., 2012. How to make a city climate-proof, addressing the urban heat island effect. *Resour. Conserv. Recycl.* 64, 30–38.
- Kotzen, B., 2003. An investigation of shade under six different tree species of the Negev desert towards their potential use for enhancing micro-climatic conditions in landscape architectural development. *J. Arid Environ.* 55, 231–274.
- Landsberg, H.E., 1981. *The Urban Climate*.
- Leitão, A.B., Miller, J., Ahern, J., McGarigal, K., 2012. *Measuring Landscapes: A Planner's Handbook*. Island press, Washington, DC.
- Li, J., Song, C., Cao, L., Zhu, F., Meng, X., Wu, J., 2011. Impacts of landscape structure on surface urban heat islands: a case study of Shanghai, China. *Remote Sens. Environ.* 115, 3249–3263.
- Li, W., Bai, Y., Chen, Q., He, K., Ji, X., Han, C., 2014. Discrepant impacts of land use and land cover on urban heat islands: a case study of Shanghai, China. *Ecol. Ind.* 47, 171–178.
- Li, W., Cao, Q., Lang, K., Wu, J., 2017. Linking potential heat source and sink to urban heat island: heterogeneous effects of landscape pattern on land surface temperature. *Sci. Total Environ.* 586, 457–465.
- Li, X., Li, W., Middel, A., Harlan, S.L., Brazel, A.J., Turner, B.L., 2016. Remote sensing of the surface urban heat island and land architecture in Phoenix, Arizona: combined effects of land composition and configuration and cadastral–demographic–economic factors. *Remote Sens. Environ.* 174, 233–243.
- Li, X., Zhou, W., Ouyang, Z., 2013. Relationship between land surface temperature and spatial pattern of greenspace: What are the effects of spatial resolution? *Landscape Urban Plann.* 114, 1–8.
- Ma, Q., Wu, J., He, C., 2016. A hierarchical analysis of the relationship between urban impervious surfaces and land surface temperatures: spatial scale dependence, temporal variations, and bioclimatic modulation. *Landscape Ecol.* 31, 1139–1153.
- Maimaitiyiming, M., Ghulam, A., Tiyip, T., Pla, F., Latorre-Carmona, P., Halik, Ü., Sawut, M., Caetano, M., 2014. Effects of green space spatial pattern on land surface temperature: implications for sustainable urban planning and climate change adaptation. *ISPRS J. Photogramm. Remote Sens.* 89, 59–66.
- Martilli, A., 2014. An idealized study of city structure, urban climate, energy consumption, and air quality. *Urban Clim.* 10, 430–446.
- McGarigal, K., Cushman, S.A., Neel, M.C., Ene, E., 2002. *FRAGSTATS: Spatial Pattern Analysis Program for Categorical Maps*.
- Miller, A., 2002. *Subset Selection in Regression*, second ed. Taylor & Francis.
- Ministry of Land and Resources of the P.R.C. (MLR). GB/T 21010-2017, 2017. *Current Land Use Classification*.
- Mirzaei, P.A., 2015. Recent challenges in modeling of urban heat island. *Sustain. Cities Soc.* 19, 200–206.
- Mottet, A., Ladet, S., Coqué, N., Gibon, A., 2006. Agricultural land-use change and its drivers in mountain landscapes: a case study in the Pyrenees. *Agric. Ecosyst. Environ.* 114, 296–310.
- NBSC (National Bureau of Statistics of China), 2016. *China City Statistical Yearbook – 2016*.
- Oke, T.R., 1988a. Street design and urban canopy layer climate. *Energy Build.* 11, 103–113.
- Oke, T.R., 1988b. The urban energy balance. *Progress in Phys. Geogr.: Earth Environ.* 12, 471–508.
- Oke, T.R., Crowther, J.M., McNaughton, K.G., Monteith, J.L., Gardiner, B., 1989. The micrometeorology of the urban forest [and discussion]. *Philos. Trans. Royal Soc. London Series B, Biol. Sci.* 324, 335–349.
- Oke, T.R., Mills, G., Christen, A., Voogt, J.A., 2017. *Urban Climates*. Cambridge University Press, Cambridge.
- Peel, M.C., Finlayson, B.L., McMahon, T.A., 2007. Updated world map of the Köppen-Geiger climate classification. *Hydrol. Earth Syst. Sci.* 11, 259–263.
- Peng, S., Piao, S., Ciais, P., Friedlingstein, P., Ottle, C., Bréon, F.-M., Nan, H., Zhou, L., Myneni, R.B., 2012. Surface urban heat island across 419 global big cities. *Environ. Sci. Technol.* 46, 696–703.
- Peng, S.S., Piao, S., Zeng, Z., Ciais, P., Zhou, L., Li, L.Z., Myneni, R.B., Yin, Y., Zeng, H., 2014. Afforestation in China cools local land surface temperature. In: *Proceedings of the National Academy of Sciences of the United States of America*, pp. 2915–2919.
- Sarrat, C., Lemonsu, A., Masson, V., Guedalia, D., 2006. Impact of urban heat island on regional atmospheric pollution. *Atmos. Environ.* 40, 1743–1758.
- Scarano, M., Mancini, F., 2017. Assessing the relationship between sky view factor and land surface temperature to the spatial resolution. *Int. J. Remote Sens.* 38, 6910–6929.
- Shahidan, M.F., Jones, P.J., Gwilliam, J., Salleh, E., 2012. An evaluation of outdoor and building environment cooling achieved through combination modification of trees with ground materials. *Build. Environ.* 58, 245–257.
- Sobrino, J.A., Jiménez-Muñoz, J.C., Paolini, L., 2004. Land surface temperature retrieval from LANDSAT TM 5. *Remote Sens. Environ.* 90, 434–440.
- Stewart, I.D., Oke, T.R., 2012. Local climate zones for urban temperature studies. *Bull. Am. Meteorol. Soc.* 93, 1879–1900.
- Theeuwes, N.E., Steeneveld, G.J., Ronda, R.J., Heusinkveld, B.G., van Hove, L.W.A., Holtslag, A.A.M., 2014. Seasonal dependence of the urban heat island on the street canyon aspect ratio. *Q. J. R. Meteorol. Soc.* 140, 2197–2210.
- Tran, D.X., Pla, F., Latorre-Carmona, P., Myint, S.W., Caetano, M., Kieu, H.V., 2017. Characterizing the relationship between land use land cover change and land surface temperature. *ISPRS J. Photogramm. Remote Sens.* 124, 119–132.
- United Nations, Department of Economic and Social Affairs, Population Division, 2014. *World Urbanization Prospects: The 2014 Revision, Highlights (ST/ESA/SER.A/352)*.
- USGS, 2016. *Landsat 8 (L8) Data Users Handbook*, Department of the Interior, U.S. Geological Survey.
- Wang, C., Middel, A., Myint, S.W., Kaplan, S., Brazel, A.J., Lukaszczuk, J., 2018. Assessing local climate zones in arid cities: the case of Phoenix, Arizona and Las Vegas, Nevada. *ISPRS J. Photogramm. Remote Sens.* 141, 59–71.
- Wang, Y., Chen, L., Kubota, J., 2016. The relationship between urbanization, energy use and carbon emissions: evidence from a panel of Association of Southeast Asian Nations (ASEAN) countries. *J. Cleaner Prod.* 112, 1368–1374.
- Weng, Q., 2009. Thermal infrared remote sensing for urban climate and environmental studies: methods, applications, and trends. *ISPRS J. Photogramm. Remote Sens.* 64, 335–344.
- Weng, Q., Liu, H., Liang, B., Lu, D., 2008. The spatial variations of urban land surface temperatures: pertinent factors, zoning effect, and seasonal variability. *IEEE J. Sel. Top. Appl. Earth Obs. Remote Sens.* 1, 154–166.
- Weng, Q., Lu, D., Schubring, J., 2004. Estimation of land surface temperature–vegetation abundance relationship for urban heat island studies. *Remote Sens. Environ.* 89, 467–483.
- Wong, J.K.W., Lau, L.S.-K., 2013. From the 'urban heat island' to the 'green island'? A preliminary investigation into the potential of retrofitting green roofs in Mongkok district of Hong Kong. *Habitat Int.* 39, 25–35.
- Wong, P.P.-Y., Lai, P.-C., Low, C.-T., Chen, S., Hart, M., 2016. The impact of environmental and human factors on urban heat and microclimate variability. *Build. Environ.* 95, 199–208.
- Wu, C.D., Lung, S.C.C., 2016. Application of 3-D urbanization index to assess impact of urbanization on air temperature. *Sci. Rep.* 6, 24351.
- Xie, Q., Zhou, Z., Teng, M., Wang, P., 2012. A multi-temporal Landsat TM data analysis of the impact of land use and land cover changes on the urban heat island effect. *J. Food Agric. Environ.* 10, 803–809.
- Yang, F., Qian, F., Lau, S.S.Y., 2013. Urban form and density as indicators for summertime outdoor ventilation potential: a case study on high-rise housing in Shanghai. *Build. Environ.* 70, 122–137.
- Yang, L., Niyogi, D., Tewari, M., Aliaga, D., Chen, F., Tian, F., Ni, G., Yang, L., Niyogi, D., Tewari, M., 2016. Contrasting impacts of urban forms on the future thermal environment: example of Beijing metropolitan area. *Environ. Res. Lett.* 11.
- Yang, Q., Huang, X., Li, J., 2017. Assessing the relationship between surface urban heat islands and landscape patterns across climatic zones in China. *Sci. Rep.* 7, 9337.
- Yang, Q., Huang, X., Tang, Q., 2019. The footprint of urban heat island effect in 302 Chinese cities: temporal trends and associated factors. *Sci. Total Environ.* 655, 652–662.
- Yang, X., Yao, L., Jin, T., Peng, L.L.H., Jiang, Z., Hu, Z., Ye, Y., 2018. Assessing the thermal behavior of different local climate zones in the Nanjing metropolis, China. *Build. Environ.* 137, 171–184.
- Yuan, F., Bauer, M.E., 2007. Comparison of impervious surface area and normalized difference vegetation index as indicators of surface urban heat island effects in Landsat imagery. *Remote Sens. Environ.* 106, 375–386.
- Zakšek, K., Oštir, K., Kokalj, Ž., 2011. Sky-view factor as a relief visualization technique. *Remote Sensing* 3.
- Zhang, X., Du, S., Wang, Q., 2017a. Hierarchical semantic cognition for urban functional zones with VHR satellite images and POI data. *ISPRS J. Photogramm. Remote Sens.* 132, 170–184.
- Zhang, Y., Murray, A.T., Ji, B.L.T., 2017b. Optimizing green space locations to reduce daytime and nighttime urban heat island effects in Phoenix, Arizona. *Landscape Urban Plann.* 165, 162–171.
- Zhao, L., Lee, X., Smith, R.B., Oleson, K., 2014. Strong contributions of local background climate to urban heat islands. *Nature* 511, 216–219.
- Zhou, B., Rybski, D., Kropp, J.P., 2017a. The role of city size and urban form in the surface urban heat island. *Sci. Rep.* 7, 4791.
- Zhou, W., Huang, G., Cadenasso, M.L., 2011. Does spatial configuration matter? Understanding the effects of land cover pattern on land surface temperature in urban landscapes. *Landscape Urban Plann.* 102, 54–63.
- Zhou, W., Pickett, S.T.A., Cadenasso, M.L., 2017b. Shifting concepts of urban spatial heterogeneity and their implications for sustainability. *Landscape Ecol.* 32, 15–30.
- Zhou, W., Qian, Y., Li, X., Li, W., Han, L., 2014. Relationships between land cover and the surface urban heat island: seasonal variability and effects of spatial and thematic resolution of land cover data on predicting land surface temperatures. *Landscape Ecol.* 29, 153–167.
- Zhou, W., Wang, J., Cadenasso, M.L., 2017c. Effects of the spatial configuration of trees on urban heat mitigation: a comparative study. *Remote Sens. Environ.* 195, 1–12.
- Zhou, Y., Weng, Q., Gurney, K.R., Shuai, Y., Hu, X., 2012. Estimation of the relationship between remotely sensed anthropogenic heat discharge and building energy use. *ISPRS J. Photogramm. Remote Sens.* 67, 65–72.